International Journal of Innovative Computing, Information and Control
Volume **17**, Number **2**, April **2021**

 ISSN 1349-4198
pp. 581–593

INTEGRATED GUIDANCE AND CONTROL FOR MISSILES WITH THREE-DIMENSIONAL IMPACT ANGLE CONSTRAINED

Huaming Qian and Tong Li*

College of Intelligent Systems Science and Engineering
Harbin Engineering University
No. 145, Nantong Street, Nangang District, Harbin 150001, P. R. China
*Corresponding author: litong256@hrbeu.edu.cn

Received September 2020; revised January 2021

Abstract. *This paper investigates the robust three-dimensional integrated guidance and control law for the missile with the constraint of the input saturation and impact angle. Based on the dynamic equation of the relative motion of missile-target in three-dimensional plane, the integrated guidance and control law with the constraint of the impact angle can deal with the external disturbances with unknown bounds by using the adaptive control. To deal with the problem of the input saturation, an auxiliary system is introduced to the integrated guidance and control. Finally, the effectiveness of the designed law is verified through the Lyapunov theory and numerical simulations.*
Keywords: Integrated guidance and control, Input saturation, Sliding mode control, Adaptive control, Robust control

1. **Introduction.** In the traditional missile guidance and control methods, the guidance and control systems are regarded as two different processes. The guidance system is designed as an outer loop that generates an acceleration tracked by the inner loop autopilot which is usually designed without considering the position and speed information between the missile and target [1,2]. However, the relative distance between the missile and target becoming smaller and the rapid change of the relative geometry may lead to the system performance degradation, and even the failure of the separation design method. In order to avoid these shortcomings, the integrated guidance and control design has been investigated by domestic and international scholars [3,4]. The θ-D method [5], sliding mode control [6,7], second-order sliding mode control [8], and dynamic surface control [9] have been widely used in the design of the integrated guidance and control algorithm. To make the missile achieve the all-round attack ability, Wang et al. [10] gave an integrated guidance and control method with the impact angle constrained. To improve the damage ability to the target, He et al. [11] designed an integrated guidance and control law with the impact angle constraint to deal with the problem of intercepting unknown maneuvering targets. To deal with actuator saturation constraints in real systems, Ma et al. [9] investigated an integrated guidance and control law by using the dynamic surface control, backstepping control and adaptive neural network.

The approaches mentioned above are to decouple the missile-target engagement dynamics into two mutually perpendicular planes, and then design the integrated guidance and control law for the two planes respectively. However, the cross-coupling effects between the two planes are neglected in this simplified method, which will make the system precision reduce. Therefore, in order to improve the performance of the missile system, various integrated guidance and control techniques in three-dimensional space have been

DOI: 10.24507/ijicic.17.02.581

investigated, such as the dynamic surface control [12], back-stepping control [13], sliding mode control [14], and high-order sliding mode control [15]. In modern war, it not only requires the missile to hit the target with high accuracy, but also requires the missile achieving the all-round attack ability to the target from different angles to improve the damage ability to the target. To solve the problem, the three-dimensional integrated guidance and control law with the impact angle constraint has been studied for the missile system by numerous scholars [16-18]. Wang and Wang [16] designed a partial integrated guidance and control law for an interception with terminal impact angle constraints and aerodynamic uncertainties. Liu et al. [17] proposed a three-dimensional integrated guidance and control law for a class of bank-to-turn aircraft with fixed target and constrained terminal flight angles by using the dynamic surface control and back-stepping method. Lai et al. [18] gave an adaptive finite-time dynamic surface control law with the impact angle constrained for a surface-to-air skid-to-turn missile intercepting a head-on maneuvering target.

It is obvious that the missile usually suffers from the input saturation problem which may cause unacceptable performance degradation of the missile system [19-21]. In order to deal with the physical constraints of actuators, anti-saturation integrated guidance and control laws have been studied for the missile by numerous scholars. Liu et al. [22] designed an integrated guidance and control law for missiles attacking manoeuvring target, in which an auxiliary system was introduced to handle the input saturation. Zhou and Xu [23] investigated an anti-saturation guidance law with autopilot dynamics by using the block dynamic surface control. Wang et al. [24,25] gave an anti-saturation integrated guidance and control law with the impact angle constraint by using the Nussbaum function and dynamic surface control. Liu et al. [26] proposed an anti-saturation integrated guidance and control approach by using the dynamic surface control and barrier Lyapunov function.

Though some integrated guidance and control laws can deal with the problem of input saturation, it is still one of challenging problems to design the robust anti-saturation three-dimensional integrated guidance and control laws for the missile system with the impact angle constraint. To deal with the problem, this paper designs a robust anti-saturation three-dimensional integrated guidance and control law by using the adaptive control, sliding mode control and auxiliary system. The exact contributions of current paper are concluded as follows.

i) The three-dimensional integrated guidance and control law can deal with the external disturbances with unknown bounds by using the adaptive control.

ii) By using the auxiliary system, the three-dimensional integrated guidance and control law can deal with the input saturation.

iii) The robust three-dimensional integrated guidance and control law is designed for the missile system which can deal with the impact angle constraint and input saturation simultaneously.

The rest of this paper is divided into the following sections. The integrated guidance and control system model is given in Section 2. In Section 3, the robust integrated guidance and control law and stability analysis are given. In Section 4, simulation results are presented to validate the effectiveness of the law. Finally, it comes to the conclusions of this paper.

2. **Preliminaries.** The relative motion between the missile and target in a three-dimensional plane is shown in Figure 1 and Figure 2. The coordinate system $Mxyz$ is parallel to the reference inertial coordinate system. $Mx_4y_4z_4$ is the line of sight coordinate system. M and T represent the center of mass for the missile and target, respectively. The dynamic

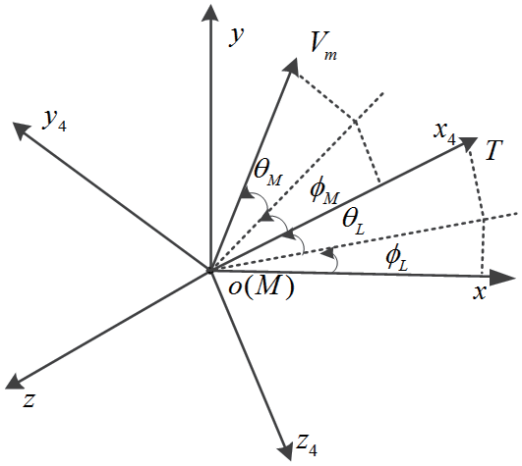

FIGURE 1. Geometry in a 3D space

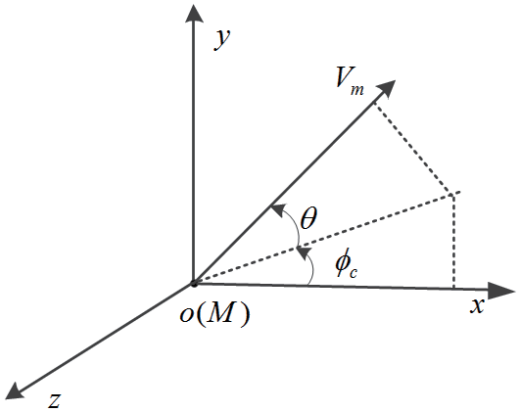

FIGURE 2. Three-dimensional geometry of missile velocity relative to inertial coordinate system

equation of the relative motion of missile-target in three-dimensional plane is given as

$$\ddot{R} - R\dot{\theta}_L^2 - R\dot{\phi}_L^2 \cos^2 \dot{\theta}_L = a_{tR} - a_{mR} \tag{1}$$

$$R\ddot{\theta}_L + 2\dot{R}\dot{\theta}_L + R\dot{\phi}_L^2 \sin\theta_L \cos\theta_L = a_{t\theta} - a_{m\theta} \tag{2}$$

$$-R\ddot{\phi}_L \cos\theta_L - 2\dot{R}\dot{\phi}_L \cos\theta_L + 2R\dot{\theta}_L\dot{\phi}_L \sin\theta_L = a_{t\phi} - a_{m\phi} \tag{3}$$

where R is the distance between the missile and target, θ_L and ϕ_L denote the line-of-sight elevation angle and line-of-sight azimuth angle, respectively, $\boldsymbol{a}_T = [a_{tR}, a_{t\theta}, a_{t\phi}]^{\mathrm{T}}$ and $\boldsymbol{a}_M = [a_{mR}, a_{m\theta}, a_{m\phi}]^{\mathrm{T}}$ are the target acceleration and missile acceleration along the line of sight coordinate system, respectively.

Since the acceleration of the missile is usually provided by the aerodynamic force in the terminal guidance segment, the relationship between the acceleration of the missile and the aerodynamic force should be further considered. The aerodynamic force on the missile in the velocity coordinate system can be obtained

$$a_{mz} = \frac{Z}{m} \tag{4}$$

$$a_{my} = \frac{Y}{m} \tag{5}$$

$$Y = qS\left(c_y^{\alpha}\alpha + c_y^{\beta}\beta + c_y^{\delta_z}\delta_z\right) \tag{6}$$

$$Z = qS\left(c_z^{\alpha}\alpha + c_z^{\beta}\beta + c_z^{\delta_y}\delta_y\right) \tag{7}$$

where a_{mz} and a_{my} are the missile acceleration along the velocity coordinate system, m denotes the mass of the missile, ρ is the air density, Y and Z are lift and side forces, V_m is the velocity of the missile, $q = \frac{1}{2}\rho V_m^2$ denotes the dynamic pressure, S is the reference area of the missile, α, β, δ_x, δ_y, δ_z are the angle of attack, angle of sideslip, aileron, rudder, and elevator deflections, respectively, c_y^{α}, c_y^{β}, $c_y^{\delta_z}$ are the partial derivatives of lift coefficient, and c_z^{α}, c_z^{β}, $c_z^{\delta_y}$ are the partial derivatives of the side force coefficient.

Combined with (2), (3), (6) and (7), it can get

$$\begin{aligned}\ddot{\theta}_L = &-\dot{\phi}_L^2 \sin\theta_L \cos\theta_L - \frac{2\dot{R}\dot{\theta}_L}{R} + M_1 mg\cos\theta - M_1\left(Y\cos\left(\gamma_V\right) - Z\sin\left(\gamma_V\right)\right)\\ &- \frac{\sin\theta_L \sin\left(\phi_L - \phi_c\right)}{mR}\left(Y\sin\left(\gamma_V\right) - Z\cos\left(\gamma_V\right)\right) + d_{\theta L}\end{aligned} \tag{8}$$

$$\begin{aligned}\ddot{\phi}_L = &-\frac{2\dot{R}\dot{\phi}_L}{R} + 2\dot{\theta}_L\dot{\phi}_L\tan\theta_L + M_2 mg\cos\theta - M_2\left(Y\cos\left(\gamma_V\right) - Z\sin\left(\gamma_V\right)\right)\\ &+ \frac{qSc_z^{\beta}\cos\left(\phi_L - \phi_c\right)}{mR\cos\theta_L}\left(Y\sin\left(\gamma_V\right) - Z\cos\left(\gamma_V\right)\right) + d_{\phi L}\end{aligned} \tag{9}$$

$$M_1 = \frac{\cos\theta\cos\theta_L + \sin\theta\sin\theta_L\cos\left(\phi_L - \phi_c\right)}{mR} \tag{10}$$

$$M_2 = \frac{\sin\theta\sin\left(\phi_L - \phi_c\right)}{mR\cos\theta_L} \tag{11}$$

where $d_{\theta L}$ and $d_{\phi L}$ are the interferences of the system, γ_V is the velocity bank angle, and ϕ_c is the heading angle.

Kinematics equations of the flight path angle θ and heading angle ϕ_c are shown as follows:

$$\dot{\theta} = \frac{Y\cos\gamma_V - Z\sin\gamma_V - mg\cos\theta}{mV_m} \tag{12}$$

$$\dot{\phi}_c = \frac{-Y\sin\gamma_V - Z\cos\gamma_V}{mV_m\cos\theta} \tag{13}$$

Next, the attitude kinematics equation of missile can be obtained as follows:

$$\dot{\alpha} = -\omega_x\tan\beta\cos\alpha + \omega_y\tan\beta\sin\alpha + \omega_z - \frac{Y}{mV_m\cos\beta} + \frac{g}{V_m\cos\beta}\cos\theta\cos\gamma_V \tag{14}$$

$$\dot{\beta} = \omega_x\sin\alpha + \omega_y\cos\alpha + \frac{Z}{mV_m} + \frac{g}{V_m}\cos\theta\sin\gamma_V \tag{15}$$

$$\begin{aligned}\dot{\gamma}_V = &\cos\alpha\sec\beta\omega_x - \sin\alpha\sec\beta\omega_y - \frac{\cos\theta\cos\gamma_V\tan\beta}{V_m}g\\ &+ \frac{Y\left(\tan\theta\sin\gamma_V + \tan\beta\right) + Z\tan\theta\cos\gamma_V}{mV_m}\end{aligned} \tag{16}$$

where g is the gravity acceleration, ω_x, ω_y, ω_z are the velocities of roll, yaw and pitch angle.

The attitude dynamics equation of missile can be obtained as follows:

$$\dot{\omega}_x = \frac{J_y - J_z}{J_x}\omega_z\omega_y + \frac{M_x}{J_x} \tag{17}$$

$$\dot{\omega}_y = \frac{J_z - J_x}{J_y}\omega_x\omega_z + \frac{M_y}{J_y} \tag{18}$$

$$\dot{\omega}_z = \frac{J_x - J_y}{J_z}\omega_y\omega_x + \frac{M_z}{J_z} \tag{19}$$

where J_x, J_y, J_z are the inertia moments in the direction of roll, yaw and pitch, respectively. M_x, M_y and M_z can be obtained as follows:

$$M_x = qSL\left(m_x^{\alpha}\alpha + m_x^{\beta}\beta + m_x^{\delta_x}\delta_x\right) \tag{20}$$

$$M_y = qSL\left(m_y^{\beta}\beta + m_y^{\delta_y}\delta_y\right) \tag{21}$$

$$M_z = qSL\left(m_z^{\alpha}\alpha + m_z^{\delta_z}\delta_z\right) \tag{22}$$

where L is the length of the reference. m_x^{α}, m_x^{β}, $m_x^{\delta_x}$ are partial derivatives of rolling moment coefficient, m_y^{β}, $m_y^{\delta_y}$ are partial derivatives of yawing moment coefficient, and m_z^{α}, $m_z^{\delta_z}$ are partial derivatives of pitching moment coefficient.

Combined with (8) and (9) and (14)-(22), a three-dimensional guidance and control integration model can be given as [27]

$$\dot{\boldsymbol{x}}_1 = \boldsymbol{f}_1 + \boldsymbol{b}_1\bar{\boldsymbol{x}}_2 + \boldsymbol{d}_1 \tag{23}$$

$$\dot{\boldsymbol{x}}_2 = \boldsymbol{f}_2 + \boldsymbol{b}_2\boldsymbol{x}_3 + \boldsymbol{d}_2 \tag{24}$$

$$\dot{\boldsymbol{x}}_3 = \boldsymbol{f}_3 + \boldsymbol{b}_3\mathrm{sat}(\boldsymbol{u}) + \boldsymbol{d}_3 \tag{25}$$

where $\boldsymbol{x}_1 = \begin{bmatrix} \dot{\theta}_L & \dot{\phi}_L \end{bmatrix}^{\mathrm{T}}$, $\boldsymbol{x}_2 = \begin{bmatrix} \alpha & \beta & \gamma_V \end{bmatrix}^{\mathrm{T}}$, $\boldsymbol{x}_3 = \begin{bmatrix} \omega_x & \omega_y & \omega_z \end{bmatrix}^{\mathrm{T}}$, $\bar{\boldsymbol{x}}_2 = \begin{bmatrix} \alpha & \beta \end{bmatrix}^{\mathrm{T}}$, $\boldsymbol{u} = \begin{bmatrix} \delta_x & \delta_y & \delta_z \end{bmatrix}^{\mathrm{T}}$, $\boldsymbol{d}_1$, $\boldsymbol{d}_2$, $\boldsymbol{d}_3$ are the total interferences of the system. $\boldsymbol{b}_1$, $\boldsymbol{b}_2$, $\boldsymbol{b}_3$, $\boldsymbol{f}_1$, $\boldsymbol{f}_2$ and $\boldsymbol{f}_3$ can be obtained as follows:

$$\boldsymbol{b}_1 = \begin{bmatrix} -M_1qSc_y^{\alpha} & -\dfrac{qSc_z^{\beta}\sin\theta_L\sin(\phi_L-\phi_c)}{mR} \\ -M_2qSc_y^{\alpha} & \dfrac{qSc_z^{\beta}\cos(\phi_L-\phi_c)}{mR\cos\theta_L} \end{bmatrix} \tag{26}$$

$$\boldsymbol{b}_2 = \begin{bmatrix} -\tan\beta\cos\alpha & \tan\beta\sin\alpha & 1 \\ \sin\alpha & \cos\alpha & 0 \\ \cos\alpha\sec\beta & -\sin\alpha\sec\beta & 0 \end{bmatrix} \tag{27}$$

$$\boldsymbol{b}_3 = \begin{bmatrix} \dfrac{qSLm_x^{\delta_x}}{J_x} & 0 & 0 \\ 0 & \dfrac{qSLm_y^{\delta_y}}{J_y} & 0 \\ 0 & 0 & \dfrac{qSLm_z^{\delta_z}}{J_z} \end{bmatrix} \tag{28}$$

$$\boldsymbol{f}_1 = \begin{bmatrix} -\dfrac{2\dot{R}}{R}\dot{\theta}_L - \dot{\phi}_L^2\sin\theta_L\cos\theta_L + M_1mg\cos\theta \\ -\dfrac{2\dot{R}}{R}\dot{\phi}_L + 2\dot{\theta}_L\dot{\phi}_L\tan\theta_L + M_2mg\cos\theta \end{bmatrix} \tag{29}$$

$$\boldsymbol{f}_2 = \begin{bmatrix} -\dfrac{qS\left(c_y^{\alpha}\alpha + c_y^{\beta}\beta\right)}{mV\cos\beta} + \dfrac{g}{V\cos\beta}\cos\theta\cos\gamma_V \\ \dfrac{qS\left(c_z^{\alpha}\alpha + c_z^{\beta}\beta\right)}{mV} + \dfrac{g}{V}\cos\theta\sin\gamma_V \\ -\dfrac{\cos\theta\cos\gamma_V\tan\beta}{V}g + \dfrac{\left(qS\left(c_y^{\alpha}\alpha + c_y^{\beta}\beta\right)\right)\left(\tan\theta\sin\gamma_V + \tan\beta\right) + \left(qS\left(c_z^{\alpha}\alpha + c_z^{\beta}\beta\right)\right)\tan\theta\cos\gamma_V}{mV} \end{bmatrix}^{\mathrm{T}} \tag{30}$$

$$\boldsymbol{f}_3 = \begin{bmatrix} \dfrac{J_y - J_z}{J_x}\omega_z\omega_y + \dfrac{qSL\left(m_x^{\alpha}\alpha + m_x^{\beta}\beta\right)}{J_x} \\ \dfrac{J_z - J_x}{J_y}\omega_x\omega_z + \dfrac{qSLm_y^{\beta}\beta}{J_y} \\ \dfrac{J_x - J_y}{J_z}\omega_y\omega_x + \dfrac{qSLm_z^{\alpha}\alpha}{J_z} \end{bmatrix} \tag{31}$$

Remark 2.1. *Due to the limitation of the missile seeker itself and the size of the target itself, R is not equal to zero when the missile hits its target. R satisfies $R_0 < R < R(0)$, in which R_0 is the minimum operating distance of the seeker and $R(0)$ is the initial value of R. In addition, $\theta_L = \pm\frac{\pi}{2}$ is a singular point, which can be avoided by selecting an appropriate reference coordinate system in the terminal guidance segment. So, $\boldsymbol{b}_1$, $\boldsymbol{b}_2$ and $\boldsymbol{b}_3$ are invertible matrix.*

Control objective: This paper is working on integrated guidance and control for the system (23)-(25). Assuming that θ_{Lf} and ϕ_{Lf} are the desired line-of-sight elevation angle and line-of-sight azimuth angle, the design goals of this paper are $\dot{\theta}_L \to 0$, $\dot{\phi}_L \to 0$, $\theta_L \to \theta_{Lf}$, $\phi_L \to \phi_{Lf}$ when the system has actuator saturation and external disturbances.

3. Main Results.

In this section, STT control is adopted, which means to maintain the velocity inclination angle during the interception process $\gamma_V = 0$. To facilitate the integrated guidance and control law design, the following assumption is given.

Assumption 3.1. *The total interferences of the system $\boldsymbol{d}_1$, $\boldsymbol{d}_2$, $\boldsymbol{d}_3$ are satisfied $\|\boldsymbol{d}_1\| \leq d_{1\max}$, $\|\boldsymbol{d}_2\| \leq d_{2\max}$, $\|\boldsymbol{d}_3\| \leq d_{3\max}$, where $d_{1\max}$, $d_{2\max}$, $d_{3\max}$ are unknown positive constants.*

To illustrate the robust control procedures, the design of the integrated guidance and control law is elaborated in detail.

Step 1: Designing the virtual controller for the system (23)

The system errors are defined as

$$\boldsymbol{e} = \begin{bmatrix} \theta_L & \phi_L \end{bmatrix}^{\mathrm{T}} - \begin{bmatrix} \theta_{Lf} & \phi_{Lf} \end{bmatrix}^{\mathrm{T}} \tag{32}$$

$$\boldsymbol{x}_1 = \dot{\boldsymbol{e}} \tag{33}$$

The sliding mode surface $\boldsymbol{S}_1$ is designed as

$$\boldsymbol{S}_1 = \boldsymbol{x}_1 + k_0\boldsymbol{e} \tag{34}$$

Taking the derivative of (34) with respect to time, it can get

$$\dot{\boldsymbol{S}}_1 = \boldsymbol{f}_1 + \boldsymbol{b}_1\bar{\boldsymbol{x}}_2 + \boldsymbol{d}_1 + k_0\boldsymbol{x}_1 \tag{35}$$

Ignoring the system disturbance $\boldsymbol{d}_1$ which is dealt with below, the virtual controller is given as

$$\boldsymbol{Z}_2 = \boldsymbol{b}_1^{-1}\left(-\boldsymbol{f}_1 - k_1\boldsymbol{S}_1 - k_0\boldsymbol{x}_1\right) \tag{36}$$

where k_1 is a positive constant. If $\boldsymbol{Z}_2 = \bar{\boldsymbol{x}}_2$, substituting (36) into Equation (35) it can get

$$\dot{\boldsymbol{S}}_1 = -k_1\boldsymbol{S}_1 + \boldsymbol{d}_1 \tag{37}$$

Then it can get $\boldsymbol{S}_1 \to 0$.

Step 2: Designing the virtual controller for the system (24)

In order to realize $\boldsymbol{Z}_2$ tracking $\bar{\boldsymbol{x}}_2$, the sliding mode surface is defined

$$\boldsymbol{S}_2 = \begin{bmatrix} s_{21} \\ s_{22} \\ s_{23} \end{bmatrix} = \boldsymbol{x}_2 - \begin{bmatrix} \boldsymbol{Z}_2 \\ 0 \end{bmatrix} \tag{38}$$

Take the derivative of (38) with respect to time and get

$$\dot{\boldsymbol{S}}_2 = \boldsymbol{f}_2 + \boldsymbol{b}_2\boldsymbol{x}_3 + \boldsymbol{d}_2 - \begin{bmatrix} \dot{\boldsymbol{Z}}_2 \\ 0 \end{bmatrix} \tag{39}$$

Ignoring the system disturbance $\boldsymbol{d}_2$ which is dealt with below, the virtual controller is given as

$$\boldsymbol{Z}_3 = \boldsymbol{b}_2^{-1}\left(-\boldsymbol{f}_2 - \begin{bmatrix} \boldsymbol{b}_1^{\mathrm{T}}\boldsymbol{S}_1 \\ 0 \end{bmatrix} - k_2\boldsymbol{S}_2 + \begin{bmatrix} \dot{\boldsymbol{Z}}_2 \\ 0 \end{bmatrix}\right) \tag{40}$$

where k_2 is a positive constant. If $\boldsymbol{Z}_3 = \boldsymbol{x}_3$, substituting (40) into Equation (39) it can get

$$\dot{\boldsymbol{S}}_2 = -\begin{bmatrix} \boldsymbol{b}_1^{\mathrm{T}}\boldsymbol{S}_1 \\ 0 \end{bmatrix} - k_2\boldsymbol{S}_2 + \boldsymbol{d}_2 \tag{41}$$

As $\boldsymbol{S}_1 \to 0$, it can get that $\boldsymbol{S}_2 \to 0$.

Step 3: Designing the virtual controller for the system (25)

In order to realize $\boldsymbol{Z}_3$ tracking of $\boldsymbol{x}_3$, the sliding mode surface is defined

$$\boldsymbol{S}_3 = \boldsymbol{x}_3 - \boldsymbol{Z}_3 \tag{42}$$

Take the derivative of (42) with respect to time and get

$$\dot{\boldsymbol{S}}_3 = \boldsymbol{f}_3 + \boldsymbol{b}_3\mathrm{sat}(\boldsymbol{u}) + \boldsymbol{d}_3 - \dot{\boldsymbol{Z}}_3 \tag{43}$$

In order to deal with the input saturation, the saturation error is defined as

$$\Delta\boldsymbol{u} = \mathrm{sat}(\boldsymbol{u}) - \boldsymbol{u} \tag{44}$$

The system (43) can be rearranged as

$$\dot{\boldsymbol{S}}_3 = \boldsymbol{f}_3 + \boldsymbol{b}_3(\Delta\boldsymbol{u} + \boldsymbol{u}) + \boldsymbol{d}_3 - \dot{\boldsymbol{Z}}_3 \tag{45}$$

Combining the sliding mode control, adaptive control, and auxiliary system, the anti-saturation controller is designed as (46)-(51), where r_1, r_2, r_3, k_3 and k_4 are positive numbers. $\hat{D}_1$, $\hat{D}_2$ and $\hat{D}_3$ are the estimated values of $d_{1\max}$ $d_{2\max}$ and $d_{3\max}$.

$$\boldsymbol{u} = \boldsymbol{b}_3^{-1}\left(-\boldsymbol{f}_3 - \boldsymbol{b}_2^{\mathrm{T}}\boldsymbol{S}_2 - k_3\left(\boldsymbol{S}_3 - \boldsymbol{x}_e\right) + \dot{\boldsymbol{Z}}_3 - \frac{\boldsymbol{S}_3}{\|\boldsymbol{S}_3\|^2}\left(\hat{D}_1\|\boldsymbol{S}_1\| + \hat{D}_2\|\boldsymbol{S}_2\|\right)\right.$$
$$\left. - \hat{D}_3\mathrm{sgn}(\boldsymbol{S}_3)\right) \tag{46}$$

$$\dot{\boldsymbol{x}}_e = -(1/\tau)\boldsymbol{x}_e + \Delta\boldsymbol{u} \tag{47}$$

$$1/\tau = k_4 + \frac{\|\boldsymbol{S}_3\|\,\|\boldsymbol{b}_3\|\,\|\Delta\boldsymbol{u}\| + \|\Delta\boldsymbol{u}\|^2}{\|\boldsymbol{x}_e\|^2 + \gamma(\boldsymbol{x}_e)} \tag{48}$$

$$\dot{\hat{D}}_1 = r_1\|\boldsymbol{S}_1\| \tag{49}$$

$$\dot{\hat{D}}_2 = r_2\|\boldsymbol{S}_2\| \tag{50}$$

$$\dot{\hat{D}}_3 = r_3\|\boldsymbol{S}_3\| \tag{51}$$

Substituting (46) into Equation (45) it can get

$$\dot{\boldsymbol{S}}_3 = \boldsymbol{b}_3\Delta\boldsymbol{u} + \boldsymbol{d}_3 - \boldsymbol{b}_2^{\mathrm{T}}\boldsymbol{S}_2 - k_3\left(\boldsymbol{S}_3 - \boldsymbol{x}_e\right) - \frac{\boldsymbol{S}_3}{\left\|\boldsymbol{S}_3\right\|^2}\left(\hat{D}_1\left\|\boldsymbol{S}_1\right\| + \hat{D}_2\left\|\boldsymbol{S}_2\right\|\right) - \hat{D}_3\mathrm{sgn}\left(\boldsymbol{S}_3\right) \quad (52)$$

If $\Delta\boldsymbol{u} = 0$, $\boldsymbol{S}_2 \to 0$, it can get that $\boldsymbol{S}_3 \to 0$.

In conclusion, for the cascade system (23)-(25), the law (46) can be adopted to make the system meet the tracking requirements $\boldsymbol{x}_1 \to \boldsymbol{x}_{1d} = 0$.

Theorem 3.1. *Considering the system (23)-(25) satisfying Assumption 3.1, if the robust three-dimensional saturated integrated guidance and control law is given as (46), the system is asymptotically stable and* $\dot{\theta}_L \to 0$, $\dot{\phi}_L \to 0$, $\theta_L \to \theta_{Lf}$, $\phi_L \to \phi_{Lf}$.

Remark 3.1. *As the virtual control law (46) has one drawback that when* $\|\boldsymbol{S}_3\| \to 0$, $\boldsymbol{u} \to \infty$, *to deal with the problem, we improve the law (46) to be*

$$\begin{aligned}\boldsymbol{u} = {} & \boldsymbol{b}_3^{-1}\left(-\boldsymbol{f}_3 - \boldsymbol{b}_2^{\mathrm{T}}\boldsymbol{S}_2 - k_3\left(\boldsymbol{S}_3 - \boldsymbol{x}_e\right) - \hat{D}_3\mathrm{sgn}(\boldsymbol{S}_3) + \dot{\boldsymbol{Z}}_3\right) \\ & - \boldsymbol{b}_3^{-1}\begin{cases} \dfrac{\boldsymbol{S}_3}{\left\|\boldsymbol{S}_3\right\|^2}\left(\hat{D}_1\left\|\boldsymbol{S}_1\right\| + \hat{D}_2\left\|\boldsymbol{S}_2\right\|\right), & \left\|\boldsymbol{S}_3\right\|^2 > 0.001 \\ \dfrac{\boldsymbol{S}_3}{0.001}\left(\hat{D}_1\left\|\boldsymbol{S}_1\right\| + \hat{D}_2\left\|\boldsymbol{S}_2\right\|\right), & \left\|\boldsymbol{S}_3\right\|^2 \le 0.001 \end{cases}\end{aligned} \quad (53)$$

Remark 3.2. *If the robust three-dimensional integrated guidance and control law is given as (53), it can deal with the impact angle constraint and input saturation simultaneously.*

Remark 3.3. *When* $\boldsymbol{e} = 0$, *it can get* $\begin{bmatrix} \theta_L & \phi_L \end{bmatrix}^{\mathrm{T}} = \begin{bmatrix} \theta_{Lf} & \phi_{Lf} \end{bmatrix}^{\mathrm{T}}$. *It means that the robust three-dimensional saturated integrated guidance and control system implements the impact angle constraint.*

4. **Numerical Examples.** In this section, simulation results are presented to illustrate the effectiveness and applicability of the proposed robust integrated guidance and control law. In order to verify the robustness of the designed integrated guidance and control law, the target maneuvering is given as $a_{t\theta} = 3\sin(10t)$ m/s^2, $a_{t\phi} = 3\cos(10t)$ m/s^2. The parameters in the guidance and control integration model are given in Table 1 [28]. The initial scenario parameters of missile interception maneuver target are selected as shown in Table 2 [28].

TABLE 1. Initial parameters of the missile

Variable name	Variable value	Variable name	Variable value	Variable name	Variable value
S	0.42 m^2	m_z^{α}	-28.16	c_y^{α}	57.16
L	0.68 m	$m_z^{\delta_z}$	-27.92	c_y^{β}	0.08
m	1200 kg	m_y^{β}	-27.31	$c_y^{\delta_z}$	5.74
ρ	1.1558 kg/m^3	$m_y^{\delta_y}$	-26.57	c_z^{α}	-56.31
J_x	100 kg $\cdot$ m^2	m_x^{α}	0.46	c_z^{β}	-5.62
J_y	5700 kg $\cdot$ m^2	m_x^{β}	-0.37	$c_z^{\delta_y}$	0.09
J_z	5600 kg $\cdot$ m^2	$m_x^{\delta_x}$	2.12		

TABLE 2. Initial engagement parameters for the missile and target

Variable name	Variable value	Variable name	Variable value
$\theta(0)$	$45\pi/180$ rad	$z_m(0)$	0 m
$\phi_c(0)$	0 rad	V_m	1000 m/s
ω_x	0.1 rad/s	$x_t(0)$	11136 m
ω_y	0.1 rad/s	$y_t(0)$	8603 m
ω_z	0.2 rad/s	$z_t(0)$	5192.8 m
$x_m(0)$	0 m	V_t	800 m/s
$y_m(0)$	0 m		

For the system (23)-(25), the initial system parameters are selected as the above tables. The integrated guidance and control law is given as (53) where its parameters are selected as follows $k_0 = 1$, $k_1 = 1$, $k_2 = 2$, $k_3 = 2$, $k_4 = 2$, $r_1 = 0.01$, $r_2 = 0.01$ and $r_3 = 0.01$. The expected line-of-sight angles are given as $\theta_{Lf} = 30°$ and $\phi_{Lf} = -20°$. The upper limit of the control input is $u_m = 30°$.

The simulation results are shown in Figures 3-7. The distance between the missile and target R is depicted in Figure 3, from which one can deduce that the missile can hit the target with high accuracy. Figure 4 gives curves of α, β, and γ_V, from which it can get that they can converge to a very small range of zero. Figure 5 presents curves of ω_x, ω_y, and ω_z. Figure 6 presents curves of θ_L and ϕ_L, from which one can deduce that the line of sight angle can converge to the desired value. Figure 7 gives curves of δ_x, δ_y, and δ_z. Clearly, the boundary of the control input is less than 30°.

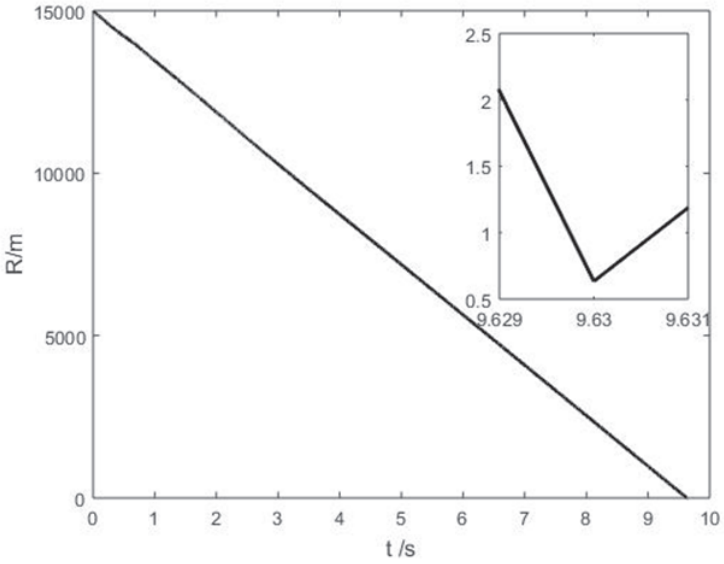

FIGURE 3. Curves of R

5. **Conclusions.** In this paper, the integrated guidance and control law for the missile has been investigated. An auxiliary system is proposed to deal with the input saturation for the missile. By using the adaptive control, the robust law can deal with the external disturbances with unknown bounds. The Lyapunov stability theory is employed to show the stability of the guidance laws. Finally, numerical simulations have been given to demonstrate the effectiveness of the proposed integrated guidance and control law. In the future, we will focus on the robust guidance law design considering the impact angle constraint, input saturation and state constraints.

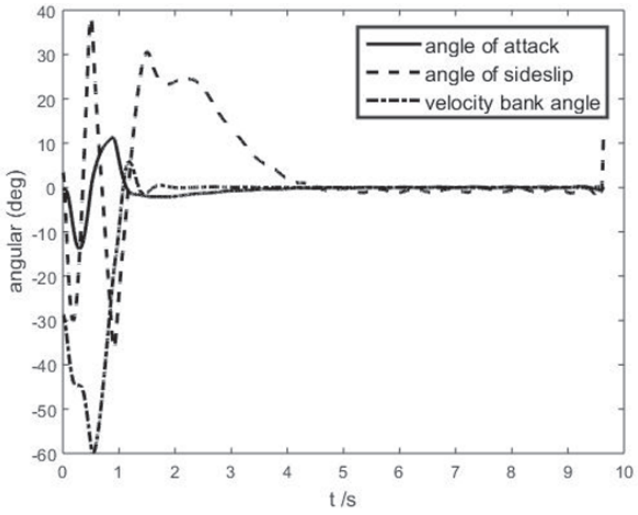

FIGURE 4. Curves of α, β, and γ_V

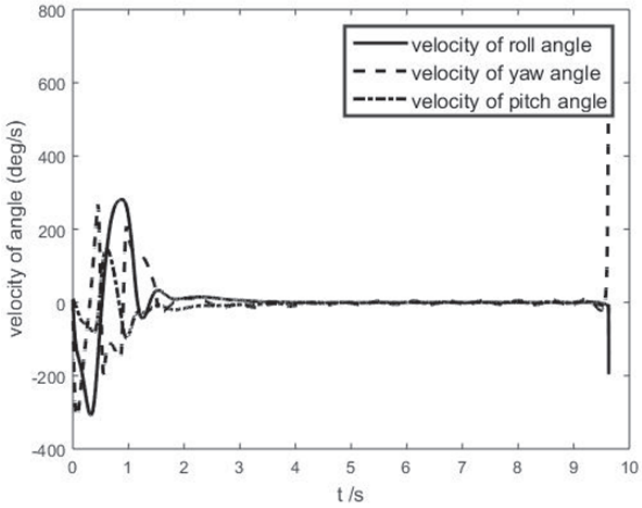

FIGURE 5. Curves of ω_x, ω_y, and ω_z

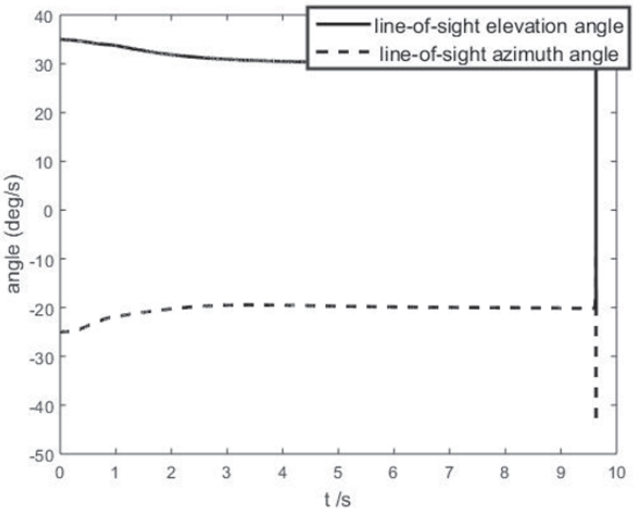

FIGURE 6. Curves of θ_L and ϕ_L

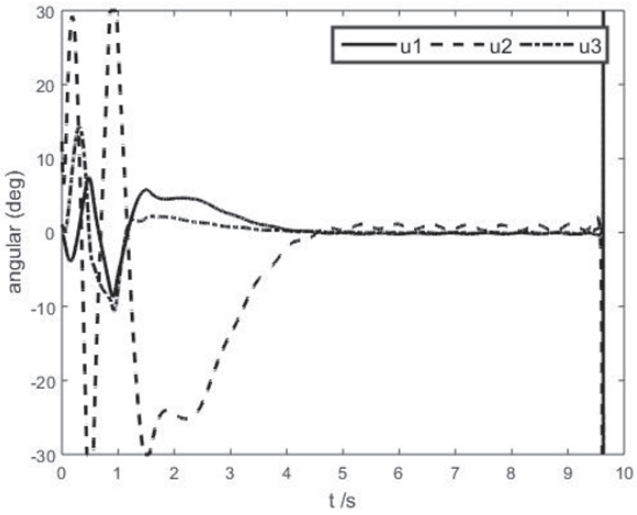

FIGURE 7. Curves of δ_x, δ_y, and δ_z

Acknowledgment. This work was partially supported by the National Natural Science Foundation of China under Grant No. 61573113. The authors also gratefully acknowledge the helpful comments and suggestions of the reviewers.

REFERENCES

[1] K. W. Lee and S. N. Singh, Longitudinal nonlinear adaptive autopilot design for missiles with control constraint, *Proc. of the Institution of Mechanical Engineers, Part G: Journal of Aerospace Engineering*, vol.232, no.9, pp.1655-1670, 2018.

[2] M. Ma, K. Zhao and S. Song, Adaptive sliding mode guidance law with prescribed performance for intercepting maneuvering target, *International Journal of Innovative Computing, Information and Control*, vol.16, no.2, pp.631-648, 2020.

[3] T. Shima, M. Idan and O. M. Golan, Sliding-mode control for integrated missile autopilot guidance, *Journal of Guidance, Control, and Dynamics*, vol.29, no.2, pp.250-260, 2006.

[4] M. Hou and G. Duan, Integrated guidance and control of homing missiles against ground fixed targets, *Chinese Journal of Aeronautics*, vol.21, no.2, pp.162-168, 2008.

[5] M. Xin, S. N. Balakrishnan and E. J. Ohlmeyer, Integrated guidance and control of missiles with θ-D method, *IFAC Proceedings Volumes*, vol.37, no.6, pp.629-634, 2004.

[6] J. Guo, Y. Xiong and J. Zhou, A new sliding mode control design for integrated missile guidance and control system, *Aerospace Science and Technology*, vol.78, pp.54-61, 2018.

[7] Y. Guo, B. Huang and A. J. Li, Integral sliding mode control for Euler-Lagrange systems with input saturation, *International Journal of Robust and Nonlinear Control*, vol.29, no.4, pp.1088-1100, 2019.

[8] Y. B. Shtessel, I. A. Shkolnikov and A. Levant, Guidance and control of missile interceptor using second-order sliding modes, *IEEE Trans. Aerospace and Electronic Systems*, vol.45, no.1, pp.110-124, 2009.

[9] J. Ma, H. Guo and P. Li, Adaptive integrated guidance and control design for a missile with input constraints, *IFAC Proceedings Volumes*, vol.46, no.20, pp.206-211, 2013.

[10] X. H. Wang, C. P. Tan and L. P. Cheng, Impact time and angle constrained integrated guidance and control with application to salvo attack, *Asian Journal of Control*, 2019.

[11] S. He, T. Song and D. Lin, Impact angle constrained integrated guidance and control for maneuvering target interception, *Journal of Guidance, Control, and Dynamics*, vol.40, no.10, pp.2653-2661, 2017.

[12] M. Hou, X. Liang and G. Duan, Adaptive block dynamic surface control for integrated missile guidance and autopilot, *Chinese Journal of Aeronautics*, vol.26, no.3, pp.741-750, 2013.

[13] C. Bao, P. Wang and G. Tang, Integrated guidance and control for hypersonic morphing missile based on variable span auxiliary control, *International Journal of Aerospace Engineering*, 2019.

[14] Z. Wang, J. Ma and J. Fu, Research on sliding mode method about three-dimensional integrated guidance and control for air-to-ground missile, *Journal of Aerospace Technology and Management*, 2019.

[15] R. Huo, X. Liu and X. Zeng, Integrated guidance and control based on high-order sliding mode method, *The 36th Chinese Control Conference (CCC)*, pp.6073-6078, 2017.
[16] X. Wang and J. Wang, Partial integrated guidance and control for missiles with three-dimensional impact angle constraints, *Journal of Guidance, Control, and Dynamics*, vol.37, no.2, pp.644-657, 2014.
[17] X. Liu, W. Huang and L. Du, Three-dimensional integrated guidance and control for BTT aircraft constrained by terminal flight angles, *The 27th Chinese Control and Decision Conference*, pp.107-112, 2015.
[18] C. Lai, W. Wang and Z. Liu, Three-dimensional impact angle constrained partial integrated guidance and control with finite-time convergence, *IEEE Access*, vol.6, pp.53833-53853, 2018.
[19] J. G. Sun, S. M. Song and H. T. Chen, Finite-time tracking control of hypersonic aircrafts with input saturation, *Proc. of the Institution of Mechanical Engineers, Part G: Journal of Aerospace Engineering*, vol.232, no.7, pp.1373-1389, 2018.
[20] Y. Guo, B. Huang and S. M. Song, Robust saturated finite-time attitude control for spacecraft using integral sliding mode, *Journal of Guidance, Control, and Dynamics*, vol.24, no.2, pp.440-446, 2019.
[21] S. Huang, M. Huang, J. Mi, L. Ma, Z. Lu and H. Su, Fuzzy control for trajectory tracking in shield tunneling, *ICIC Express Letters, Part B: Applications*, vol.10, no.7, pp.579-586, 2019.
[22] W. Liu, Y. Wei and G. R. Duan, Integrated guidance and control with input saturation and disturbance observer, *Journal of Control and Decision*, vol.5, no.3, pp.277-299, 2018.
[23] D. Zhou and B. Xu, Adaptive dynamic surface guidance law with input saturation constraint and autopilot dynamics, *Journal of Guidance, Control, and Dynamics*, pp.1155-1162, 2016.
[24] S. Wang, W. Wang and S. Xiong, Impact angle constrained three-dimensional integrated guidance and control for STT missile in the presence of input saturation, *ISA Transactions*, vol.64, pp.151-160, 2016.
[25] W. Wang, S. Xiong and S. Wang, Three dimensional impact angle constrained integrated guidance and control for missiles with input saturation and actuator failure, *Aerospace Science and Technology*, vol.53, pp.169-187, 2016.
[26] W. Liu, Y. Wei and G. Duan, Barrier Lyapunov function-based integrated guidance and control with input saturation and state constraints, *Aerospace Science and Technology*, vol.84, pp.845-855, 2019.
[27] H. Yan and H. B. Ji, Guidance laws based on input-to-state stability and high-gain observers, *IEEE Trans. Aerospace and Electronic Systems*, vol.48, no.3, pp.2518-2529, 2012.
[28] S. He, W. Wang and J. Wang, Three-dimensional multivariable integrated guidance and control design for maneuvering targets interception, *Journal of the Franklin Institute*, vol.353, no.16, pp.4330-4350, 2016.

Appendix. The proof of **Theorem 3.1**

Proof: The Lyapunov function V is chosen as (54), where $\tilde{D}_i = D_i - \hat{D}_i$, $(i = 1, 2, 3)$

$$V = \frac{1}{2}\sum_{i=1}^{3} \boldsymbol{S}_i^{\mathrm{T}}\boldsymbol{S}_i + \frac{1}{2r_1}\tilde{D}_1^2 + \frac{1}{2r_2}\tilde{D}_2^2 + \frac{1}{2r_3}\tilde{D}_3^2 + \frac{1}{2}\boldsymbol{x}_e^{\mathrm{T}}\boldsymbol{x}_e \tag{54}$$

Taking the time derivative of V yields

$$\begin{aligned}
\dot{V} &= \boldsymbol{S}_1^{\mathrm{T}}\dot{\boldsymbol{S}}_1 + \boldsymbol{S}_2^{\mathrm{T}}\dot{\boldsymbol{S}}_2 + \boldsymbol{S}_3^{\mathrm{T}}\dot{\boldsymbol{S}}_3 - \frac{1}{r_1}\tilde{D}_1\dot{\hat{D}}_1 - \frac{1}{r_2}\tilde{D}_2\dot{\hat{D}}_2 - \frac{1}{r_3}\tilde{D}_3\dot{\hat{D}}_3 + \boldsymbol{x}_e^{\mathrm{T}}\dot{\boldsymbol{x}}_e \\
&= \boldsymbol{S}_1^{\mathrm{T}}\left(\boldsymbol{f}_1 + \boldsymbol{b}_1\bar{\boldsymbol{x}}_2 + \boldsymbol{d}_1 + k_0\boldsymbol{x}_1\right) + \boldsymbol{S}_2^{\mathrm{T}}\left(\boldsymbol{f}_2 + \boldsymbol{b}_2\boldsymbol{x}_3 + \boldsymbol{d}_2 - \begin{bmatrix} \dot{\boldsymbol{Z}}_2 \\ 0 \end{bmatrix}\right) \\
&\quad + \boldsymbol{S}_3^{\mathrm{T}}\left(\boldsymbol{f}_3 + \boldsymbol{b}_3\mathrm{sat}(\boldsymbol{u}) + \boldsymbol{d}_3 - \dot{\boldsymbol{Z}}_3\right) - \frac{1}{r_1}\tilde{D}_1\dot{\hat{D}}_1 - \frac{1}{r_2}\tilde{D}_2\dot{\hat{D}}_2 - \frac{1}{r_3}\tilde{D}_3\dot{\hat{D}}_3 + \boldsymbol{x}_e^{\mathrm{T}}\dot{\boldsymbol{x}}_e \\
&= \boldsymbol{S}_1^{\mathrm{T}}\left(\boldsymbol{f}_1 + \boldsymbol{b}_1\left(\boldsymbol{Z}_2 + \begin{bmatrix} s_{21} \\ s_{22} \end{bmatrix}\right) + \boldsymbol{d}_1 + k_0\boldsymbol{x}_1\right) \\
&\quad + \boldsymbol{S}_2^{\mathrm{T}}\left(\boldsymbol{f}_2 + \boldsymbol{b}_2\left(\boldsymbol{S}_3 + \boldsymbol{Z}_3\right) + \boldsymbol{d}_2 - \begin{bmatrix} \dot{\boldsymbol{Z}}_2 \\ 0 \end{bmatrix}\right) \\
&\quad + \boldsymbol{S}_3^{\mathrm{T}}\left(\boldsymbol{f}_3 + \boldsymbol{b}_3(\Delta\boldsymbol{u} + \boldsymbol{u}) + \boldsymbol{d}_3 - \dot{\boldsymbol{Z}}_3\right) - \frac{1}{r_1}\tilde{D}_1\dot{\hat{D}}_1 - \frac{1}{r_2}\tilde{D}_2\dot{\hat{D}}_2 - \frac{1}{r_3}\tilde{D}_3\dot{\hat{D}}_3 + \boldsymbol{x}_e^{\mathrm{T}}\dot{\boldsymbol{x}}_e
\end{aligned}$$

$$
\begin{aligned}
&= \boldsymbol{S}_1^{\mathrm{T}}\left(\boldsymbol{d}_1 - k_1\boldsymbol{S}_1\right) + \boldsymbol{S}_2^{\mathrm{T}}\left(\boldsymbol{b}_2\boldsymbol{S}_3 + \boldsymbol{d}_2 - k_2\boldsymbol{S}_2\right) + \boldsymbol{S}_3^{\mathrm{T}}\Bigg(\boldsymbol{b}_3\Delta\boldsymbol{u} + \boldsymbol{d}_3 - \boldsymbol{b}_2^{\mathrm{T}}\boldsymbol{S}_2 - k_3(\boldsymbol{S}_3 - \boldsymbol{x}_e) \\
&\quad - \frac{\boldsymbol{S}_3}{\|\boldsymbol{S}_3\|^2}\left(\hat{D}_1\|\boldsymbol{S}_1\| + \hat{D}_2\|\boldsymbol{S}_2\|\right) - \hat{D}_3\mathrm{sgn}(\boldsymbol{S}_3)\Bigg) - \frac{1}{r_1}\tilde{D}_1\dot{\hat{D}}_1 - \frac{1}{r_2}\tilde{D}_2\dot{\hat{D}}_2 - \frac{1}{r_3}\tilde{D}_3\dot{\hat{D}}_3 \\
&\quad + \boldsymbol{x}_e^{\mathrm{T}}\dot{\boldsymbol{x}}_e \\
&= -k_1\boldsymbol{S}_1^{\mathrm{T}}\boldsymbol{S}_1 - k_2\boldsymbol{S}_2^{\mathrm{T}}\boldsymbol{S}_2 - k_3\boldsymbol{S}_3^{\mathrm{T}}\boldsymbol{S}_3 + \boldsymbol{S}_3^{\mathrm{T}}\boldsymbol{b}_3\Delta\boldsymbol{u} + k_3\boldsymbol{S}_3^{\mathrm{T}}\boldsymbol{x}_e + \boldsymbol{x}_e^{\mathrm{T}}\dot{\boldsymbol{x}}_e \\
&\le -k_1\boldsymbol{S}_1^{\mathrm{T}}\boldsymbol{S}_1 - k_2\boldsymbol{S}_2^{\mathrm{T}}\boldsymbol{S}_2 - k_3\boldsymbol{S}_3^{\mathrm{T}}\boldsymbol{S}_3 + \|\boldsymbol{S}_3\|\,\|\boldsymbol{b}_3\|\,\|\Delta\boldsymbol{u}\| + k_3\|\boldsymbol{S}_3\|\,\|\boldsymbol{x}_e\| + \boldsymbol{x}_e^{\mathrm{T}}\dot{\boldsymbol{x}}_e \\
&\le -k_1\boldsymbol{S}_1^{\mathrm{T}}\boldsymbol{S}_1 - k_2\boldsymbol{S}_2^{\mathrm{T}}\boldsymbol{S}_2 - k_3\boldsymbol{S}_3^{\mathrm{T}}\boldsymbol{S}_3 + \|\boldsymbol{S}_3\|\,\|\boldsymbol{b}_3\|\,\|\Delta\boldsymbol{u}\| + \frac{k_3}{4}\|\boldsymbol{S}_3\|^2 + k_3\|\boldsymbol{x}_e\|^2 \\
&\quad + \boldsymbol{x}_e^{\mathrm{T}}\left(-\left(k_4 + \frac{\|\boldsymbol{S}_3\|\,\|\boldsymbol{b}_3\|\,\|\Delta\boldsymbol{u}\| + \|\Delta\boldsymbol{u}\|^2}{\|\boldsymbol{x}_e\|^2 + \gamma\left(\boldsymbol{x}_e\right)}\right)\boldsymbol{x}_e + \Delta\boldsymbol{u}\right) \\
&\le -k_1\boldsymbol{S}_1^{\mathrm{T}}\boldsymbol{S}_1 - k_2\boldsymbol{S}_2^{\mathrm{T}}\boldsymbol{S}_2 - k_3\boldsymbol{S}_3^{\mathrm{T}}\boldsymbol{S}_3 + \frac{k_3}{4}\|\boldsymbol{S}_3\|^2 + k_3\|\boldsymbol{x}_e\|^2 - k_4\boldsymbol{x}_e^{\mathrm{T}}\boldsymbol{x}_e - \|\Delta\boldsymbol{u}\|^2 + \boldsymbol{x}_e^{\mathrm{T}}\Delta\boldsymbol{u} \\
&\le -k_1\boldsymbol{S}_1^{\mathrm{T}}\boldsymbol{S}_1 - k_2\boldsymbol{S}_2^{\mathrm{T}}\boldsymbol{S}_2 - k_3\boldsymbol{S}_3^{\mathrm{T}}\boldsymbol{S}_3 + \frac{k_3}{4}\|\boldsymbol{S}_3\|^2 + k_3\|\boldsymbol{x}_e\|^2 - k_4\|\boldsymbol{x}_e\|^2 - \|\Delta\boldsymbol{u}\|^2 \\
&\quad + \frac{1}{4}\|\boldsymbol{x}_e\|^2 + \|\Delta\boldsymbol{u}\|^2 \\
&\le -k_1\boldsymbol{S}_1^{\mathrm{T}}\boldsymbol{S}_1 - k_2\boldsymbol{S}_2^{\mathrm{T}}\boldsymbol{S}_2 - \frac{3k_3}{4}\boldsymbol{S}_3^{\mathrm{T}}\boldsymbol{S}_3 - \left(k_4 - k_3 - \frac{1}{4}\right)\|\boldsymbol{x}_e\|^2
\end{aligned} \tag{55}
$$

So, when $V > 0$, there is $\dot{V} \le 0$, and according to Lyapunov's stability theory $\boldsymbol{S}_i$, $\tilde{D}_i$ $(i = 1, 2, 3)$ is bound, and then $\hat{D}_i$ $(i = 1, 2, 3)$ is bound.

Define $k = \min\left\{k_1, k_2, \frac{3k_3}{4}\right\}$

$$
\dot{V} \le -k\left(\|\boldsymbol{S}_1\|^2 + \|\boldsymbol{S}_2\|^2 + \|\boldsymbol{S}_3\|^2\right) - \left(k_4 - k_3 - \frac{1}{4}\right)\|\boldsymbol{x}_e\|^2 \tag{56}
$$

$$
\begin{aligned}
&\int_0^{+\infty} k\left(\|\boldsymbol{S}_1\|^2 + \|\boldsymbol{S}_2\|^2 + \|\boldsymbol{S}_3\|^2\right) + \left(k_4 - k_3 - \frac{1}{4}\right)\|\boldsymbol{x}_e(\tau)\|^2\,\mathrm{d}\tau \\
&\le \int_0^{+\infty} -\dot{V}(\tau)\mathrm{d}\tau = V(0) - V(+\infty) < +\infty
\end{aligned} \tag{57}
$$

According to Barbalat invariance principle $\boldsymbol{S}_i \to 0$ and $\boldsymbol{x}_e \to 0$.

Now, **Theorem 3.1** has been proven.